Compatibility of structural and functional materials in flowing LiPb and effect of the dissolved impurities on corrosion

Alessandro Venturini[a*], Serena Bassini[a], Chiara Ciantelli[a], Angela Fiore[a], Daniele Martelli[a], Francesca Papa[b], Marco Utili[a]

[a)] ENEA Brasimone, 40032 Camugnano, Bologna, Italy

[b)] DIAEE Department, Sapienza University of Rome, 00186, Rome, Italy

*Corresponding author: alessandro.venturini@enea.it

The LiPb loops of the WCLL BB (Water Cooled Lithium-Lead Breeding Blanket) have the primary aim of routing tritium-rich LiPb from the Breeding Blanket to the Tritium Extraction System of DEMO Reactor. Besides, the loops maintain LiPb in the desired conditions and purify it from corrosion and activated products and from helium generated by the neutron transmutation of lithium. For some of these tasks the loops need special functional materials. Among them, niobium and vanadium are widely considered for the tritium extraction technologies for their high permeability to tritium. In addition, the loops will be made of structural materials capable of withstanding the operative conditions and the aggressive environment. The current reference material for the piping is the ASTM A335 Grade P22. This paper investigates the compatibility at 500°C of niobium, vanadium and P22 with LiPb flowing at 0.5 m/s. This velocity is the maximum foreseen in the LiPb loops, while the temperature was chosen following a conservative approach, as the maximum expected temperature is 450°C in the BB and 330°C in the loops. The specimens of the three materials were exposed for 1,000, 2,000 and 4,000 hours in IELLLO LiPb facility at ENEA Brasimone Research Centre. After the exposure, the specimens were examined by SEM-EDX, both in cross-section and surface view, XRD analyses were performed in order to investigate potential corrosion compounds formed. Weight loss analyses were also performed on niobium specimens, after chemical cleaning from adherent LiPb. The analyses highlighted the impact of corrosion products and their interaction with refractory metals (Ni and Fe) and P22 steel (Cr, after redeposition).

Keywords: vanadium, niobium, P22, corrosion, LiPb, corrosion products

1. Introduction

In the Water Cooled Lithium-Lead Breeding Blanket (WCLL BB) [1], LiPb at 330ºC slowly flows through the Breeding Units and interacts with neutrons coming from the fusion reactions, generating tritium, which has to be removed from the liquid alloy to be used as a fuel for fusion. Permeator Against Vacuum is one of the candidate technologies for this task and is based on the tritium permeation through permeable membranes [2]. The candidate materials for membranes are niobium and vanadium [3]. Although mock-ups of the Tritium Extraction Unit are under manufacturing with

both niobium [4][5] and vanadium [6][4] as membrane materials, their compatibility with LiPb was studied in stagnant conditions by Feuerstein et al. [7] and Grabner et al. [8]: they deemed both elements to be very stable in LiPb up to 650°C. The solubility of V is reported to be 1.1 and 3.5 ppmw at 500°C and 600°C respectively, whereas the solubility of Nb is reported to be 0.053 ppmw at 600°C [7]. Dissolution rate were found to be about 0.01 $g/m^2 \cdot d$ at 550°C and below 0.004 $g/m^2 \cdot d$ for Nb at 600°C [8]. Studies in flowing conditions are not available for the pure elements, although Adelhelm et al. [9] and Borgstedt et al. [10] investigated the corrosion of the vanadium alloy V-3Ti-1Si in static and flowing LiPb, proving fairly good corrosion resistance.

LiPb is a corrosive fluid, whose effect on structural materials is strongly linked with its temperature, its velocity and the amount of impurities dissolved in it [11]. Many studies have been carried out in the past to investigate corrosion on austenitic [12] and ferritic/martensitic steels [13], especially on EUROFER [14], under different operative conditions. Among the structural materials of fusion interest, the behavior of P22 ferritic steel (ASTM A335 Gr. P22) has not been investigated, despite being currently considered as one of the reference material for the piping of the LiPb loops [15]. For this reason, specimens of P22 steel were also exposed to LiPb in this campaign.

Following the lack of data on the behavior of P22 and of pure vanadium and pure niobium in flowing LiPb, it was decided to perform an experimental characterization in IELLLO (Integrated European Lead Lithium LOop) at ENEA Brasimone R.C. [16]. The tests were carried out at 500°C and 0.5 m/s for exposures of 1,000, 2,000 and 4,000 hours. This velocity is the maximum foreseen in the LiPb loops of the WCLL BB, while the temperature was chosen following a conservative approach, as the WCLL LiPb systems are isothermal at 330°C (although an alternative layout of the loops with a section at 450°C is under consideration for enhanced tritium extraction efficiency).

2. Materials and Methods

2.1 Test section and specimens

The specimens were hosted in a test section, shown in Figure 1, composed of three 1” pipes bolted together in series and installed in IELLLO facility. Each pipe hosted a rod of specimens to be removed at the end of each exposure period (1,000, 2,000 and 4,000 hours). The first pipe that LiPb wets at the entrance of the test section is longer than the other two as a long dummy specimen was added to ensure fully developed flow at the location of the specimens to be characterized. The distance to develop the flow was evaluated following the criterion $x/D>10$ [18], where D is the hydraulic diameter. In order to keep this feature for the entire campaign, the longest pipe hosted the specimens for an exposure of 4,000 hours.

The specimens were kept in position by drilling a hole in the flanges of the pipes and inserting a small plate that served as blocking and centering system for the rod of specimens (Figure 3). Leaving some millimeters between the last specimen and the blocking plate allowed to avoid stresses linked with the thermal expansion of the specimens.

After removing the rod of specimens from one of the pipes, specimens are easily separated with wrenches thanks to the socket that was previously machined on one end of each specimen (Figure 3).

This system allows to untighten the specimens without the risk to damage the surfaces also in the most challenging situations (e.g. LiPb penetration in between two specimens).

Specimen geometries are shown in Figure 3. Niobium and vanadium bars were supplied by Goodfellow with nominal purity 99.9% wt. and 99.8% wt., respectively (main impurities being 255 ppm of Ta, 230 ppm of O, <100 ppm of W and 35 ppm of N for niobium and 300 ppm of Si, 70 ppm of Fe and 15 ppm of Cr for vanadium). The bars were machined to the required diameter (14 mm) by 3T Srl. P22 specimens were machined at the workshop of ENEA Brasimone R.C. starting from bars available in the warehouse. The LiPb exposed surface was 1318.8 mm^2 for the Nb and V specimens. Dummy specimens are made of AISI316L. Alumina-coated Eurofer specimens were also exposed to flowing LiPb in IELLLO facility during this campaign and their geometries are shown in Figure 3. The results for these specimens were presented at the ICFRM-20 conference [17].

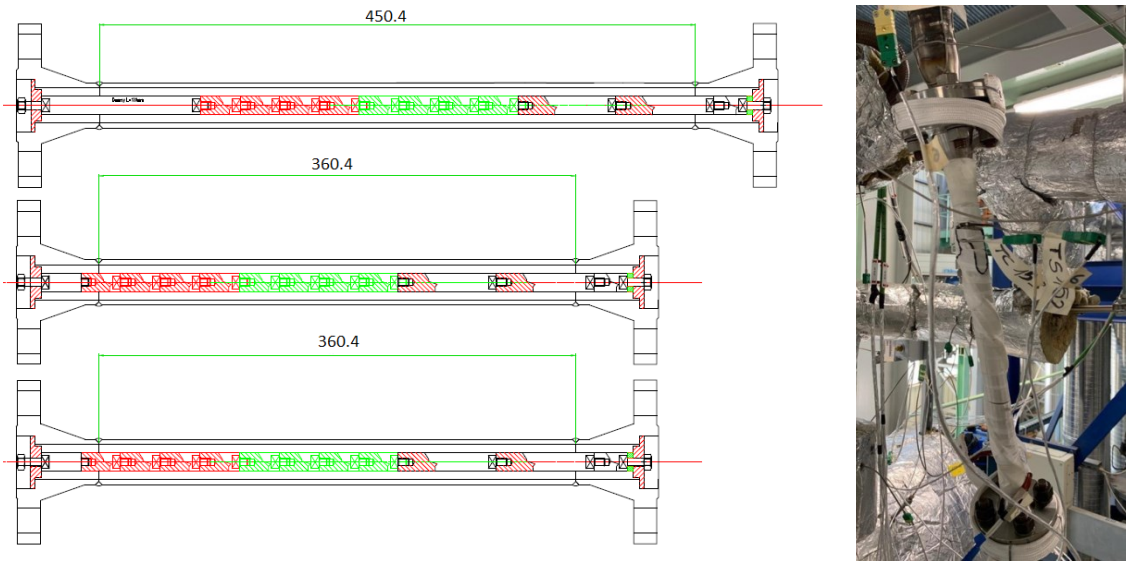

Figure 1: on the left, drawing of the three parts composing the test section and, on the right, picture of the test section before thermal insulation.

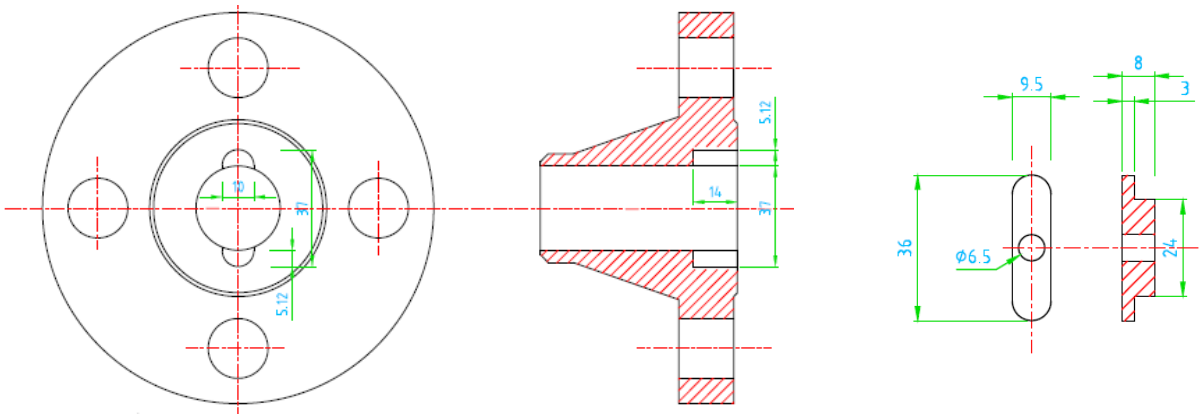

Figure 2: flange modified to hold the specimens (on the left) and centering/blocking system (on the right).

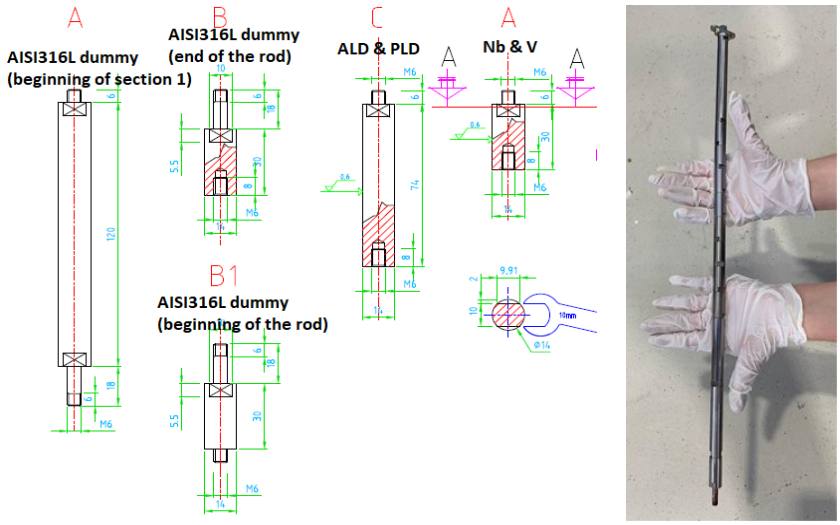

Figure 3: drawings of the specimens exposed to LiPb in this campaign (right) and picture of a rod of specimens before insertion in the test section (left).

The twelve niobium specimens were examined at SEM in cross-section and surface view and by XRD. One non-exposed specimen was also examined at SEM as a reference. Three specimens per exposure were also cleaned in a chemical solution made of acetic acid, hydrogen peroxide and ethanol (1:1:1 ratio) for 24h and then weighted. The same examinations were performed on the twelve vanadium specimens, with the exception of weight loss analysis. Vanadium is sensitive to oxidative aqueous environment and, as a consequence, it is attacked by typical chemical solutions usually used to remove residual Pb, i.e. nitric acid solutions and hydrogen peroxide solutions. For this reason a methodology to clean the V specimens is under investigation. The three P22 specimens were analyzed at SEM in cross-section and surface view.

The characterization of the samples, i.e. their morphology and their microstructure, was performed by Scanning Electron Microscopy (SEM-FEI QUANTA INSPECT-S) coupled with Energy Dispersive X-ray spectroscopy (EDX-EDAX Genesis). XRD investigations were performed by Philips X Pert-Pro diffractometer equipped with Cu Kα source.

2.2 Facility description and exposure conditions

IELLLO (Figure 4) is a large LiPb loop that was built at ENEA Brasimone R.C. in 2007 and mainly used to characterize components [19] and instrumentation [20], but also to investigate the In-box LOCA (Loss Of Coolant Accident) for the HCLL TBS (Helium Cooled Lithium-Lead Test Blanket System) with a test section named THALLIUM [21]. In the present campaign IELLLO was used to supply LiPb for specimen exposure at 500°C and 1.94 kg/s (0.5 m/s along the specimen rods). Sealed k-type thermocouples were immersed to monitor the LiPb temperature at the inlet and at the outlet of the test section: very small oscillations were measured throughout the exposure. Instead, the flow rate

was measured by the thermal mass flow meter, an instrument that was previously tested in this same facility and that proved to be reliable for being used in LiPb [20].

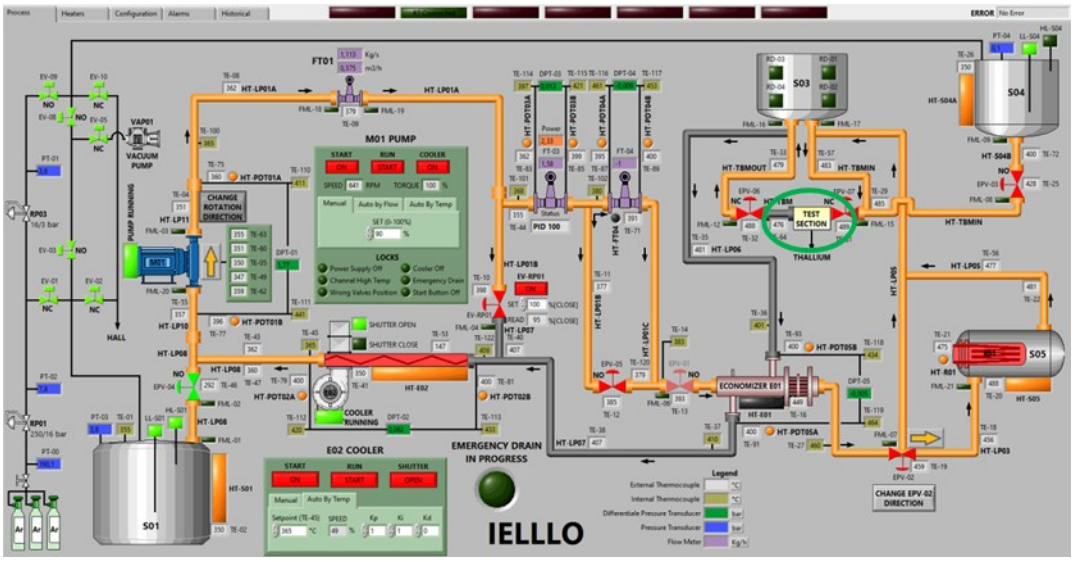

Figure 4: IELLLO layout. The test section is highlighted by a green circle.

3. Results

3.1 Weight loss on niobium specimens

The weight of the specimens before and after the exposure to flowing LiPb was measured with analytical balance with tolerance ± 0.1 mg. The results of the weight loss normalized for the exposed surface and the relative corrosion were reported in Table 1 as average values of three weighted specimens. The weight loss is slightly negative for 1,000, 2,000 and 4,000 h and indicates an increase of weight. In addition, the weight gain for 4,000 h exposed specimens is slightly higher than 1,000 and 2,000 h specimens. This slight weight gain could likely depend on traces of LiPb remained inside the screws of the specimens and also on chemical surface modification and interaction with Fe and Ni contaminants (see SEM analyses in Figure 6 hereafter). However, the final corrosion values are very low, indicating no significant corrosion/modification of Nb in the operating conditions.

Table 1: Average weight loss and corrosion of Nb specimens after exposure to LiPb with indication of the standard deviation (STD).

Time (h)	Δm (g)	STD Δm (g)	Δm/S (g/m^2)	STD Δm/S (g/m^2)	Corrosion (μm)	Density (g/cm^3)	STD corrosion (μm)
1,000	-0.0016	0.0033	-1.2	2.5	-0.1	8.57	0.3
2,000	-0.0004	0.0013	-0.3	1.0	0.0	8.57	0.1
4,000	-0.0053	0.0003	-4.0	0.3	-0.5	8.57	0.0

3.2 SEM examination

3.2.1 Niobium

Figure 5 shows cross-section SEM images at comparable magnification of Nb specimens as virgin and after exposure in flowing LiPb for all the exposure times up to 4,000 h. The specimens exposed presents a slightly increased roughness compared to that of virgin material. The bulk exhibits porosity and likely depends on the type of material production process.

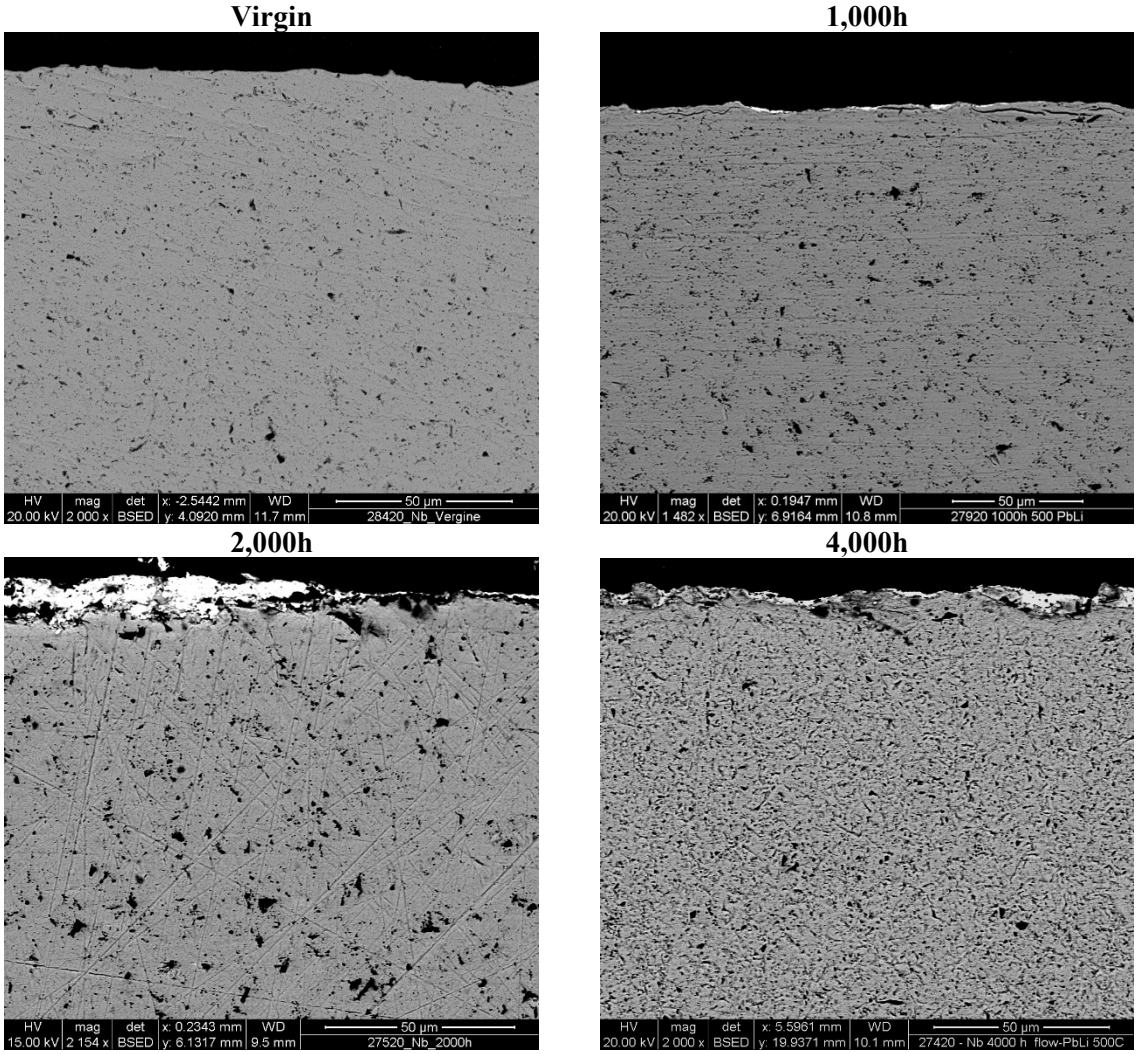

Figure 5: Cross-section SEM images at comparable magnification (1,500-2,000x) of Nb specimens as virgin and for all the exposure times up to 4,000 hours in flowing LiPb.

From the point of view of composition, various line-scans were performed at the interface to evaluate possible diffusion gradients and/or chemical modifications (Figure 6). The interface is enriched with Ni and Fe. The contamination with Ni and Fe comes from the LiPb and it is related to corrosion of the loop piping, and the surface enrichment is likely related to the formation of an intermetallic compound. In some areas, surface oxygen is also detected (line 1, 2 and 3, black areas). In other parts, the intermetallic compound is detached from the interface in the form of particles (line 3 and 4).

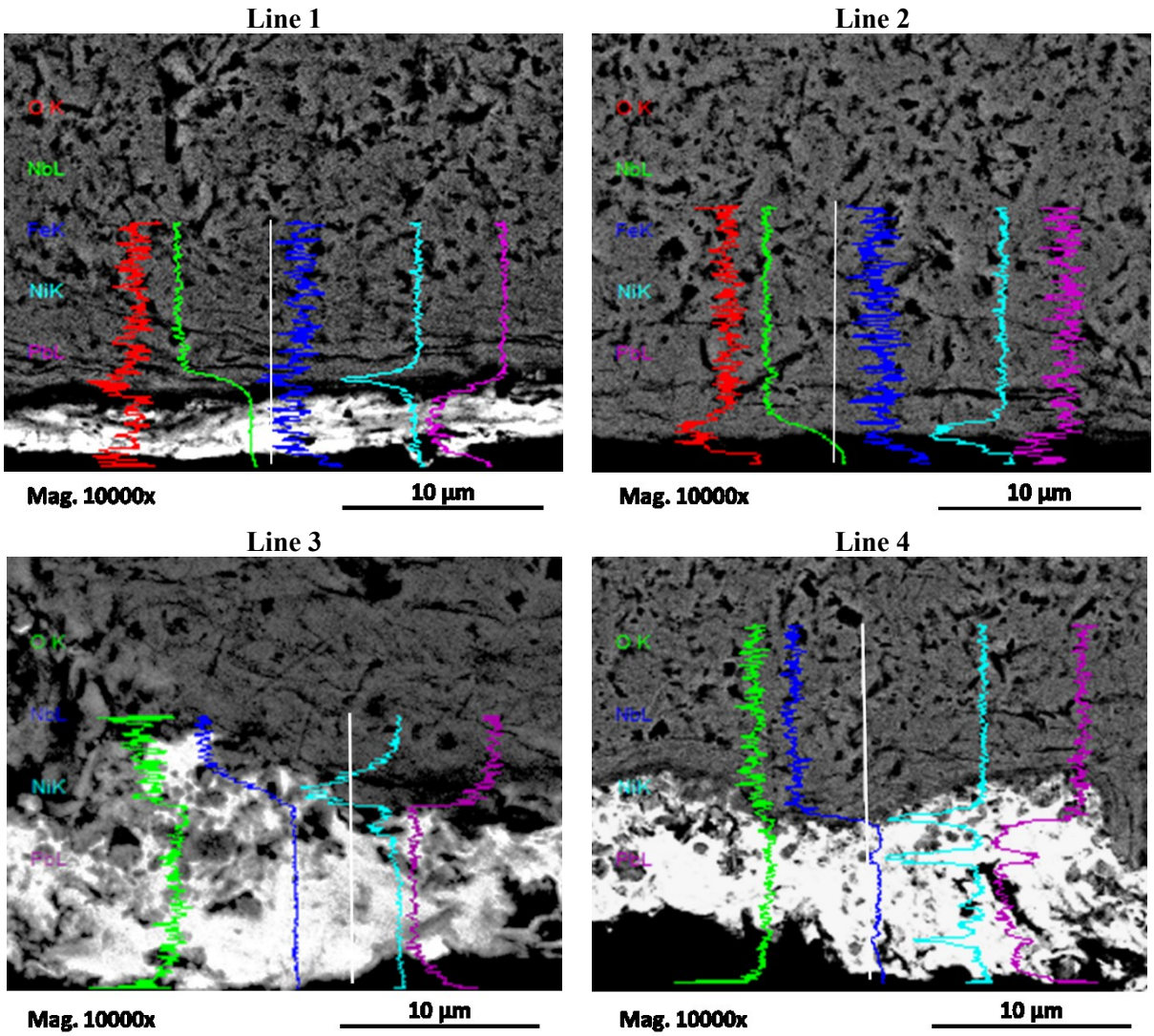

Figure 6: EDX line-scan on several areas at high magnification of the interface (10000x) in Nb specimens exposed for 4000 hours.

Surface SEM images at different magnification and EDX composition are reported in Figure 7 only for specimens exposed for 4,000 h. The surface has now a grainy/crystalline appearance and contains Nb, Ni (up to 40% wt.), Fe and O after cleaning in the chemical solution (even some traces of Pb still remained on the surface). Similar evidences were observed also for 1,000 and 2,000 h exposed specimens, but the results are not shown here for the sake of brevity. By EDX analyses performed on the specimens exposed to the various times, the amount of Ni on the surface increased with the exposure (see Table 2).

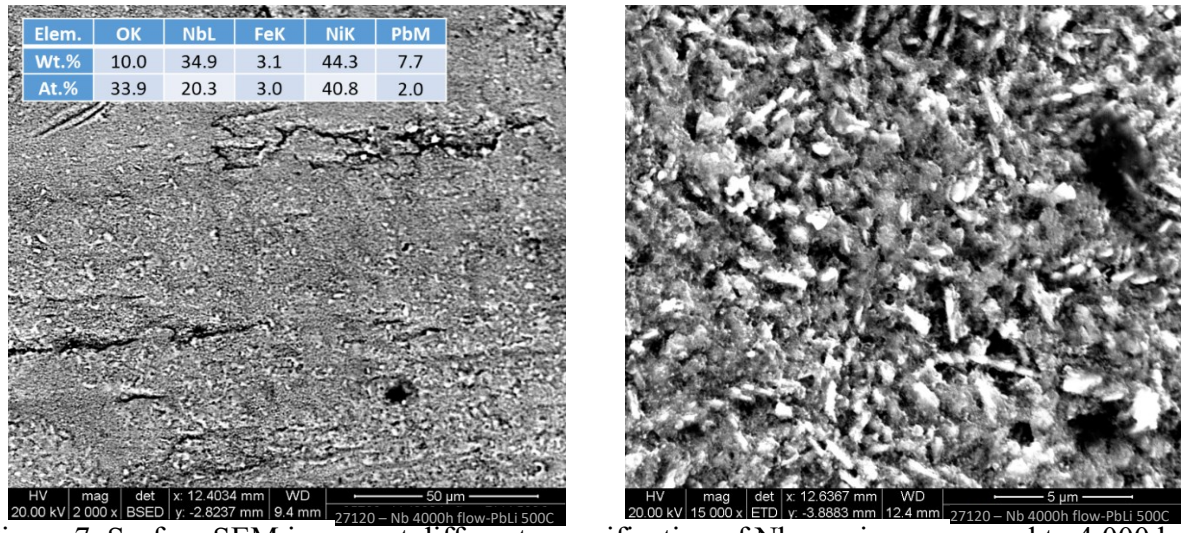

Figure 7: Surface SEM images at different magnification of Nb specimen exposed to 4,000 h in flowing LiPb, with indication of the surface composition by EDX.

3.2.2 Vanadium

Figure 8 shows cross-section SEM images at comparable magnification of V specimen as virgin and after exposure in flowing LiPb for 2,000 and 4,000 h. Going on with exposure, the specimens presents a smoother surfaces compared to that of virgin material. The bulk of the specimen exhibits porosity and likely depends on the type of material production process.

From the point of view of composition, the surface does not present a well-defined interface. EDX line-scan on high magnification images indicate the presence of a layer enriched with Ni and Fe elements at the interface (see Figure 9), as also detected in 1,000 and 2,000 h exposed specimens and likely related to the formation of intermetallics. The layer enriched by Ni and Fe is about 1.5 µm thick. In addition, the formed layer tends to be detached or dissolved during the exposure. The formation of this layer is also confirmed by EDX elemental maps in Figure 10.

Point compositional analysis by EDX confirms the presence of Ni, Fe and V in the layer at the interface (Figure 11). The content of Ni and Fe is significant (26% wt. and 6% wt. respectively) and there is also some oxygen (about 8% wt.). There is also a trace of Al inside the layer (1% wt.) and this may depend on the contamination of the LiPb inside the loop. The Si content is likely related to the preparation of the samples for the SEM examination.

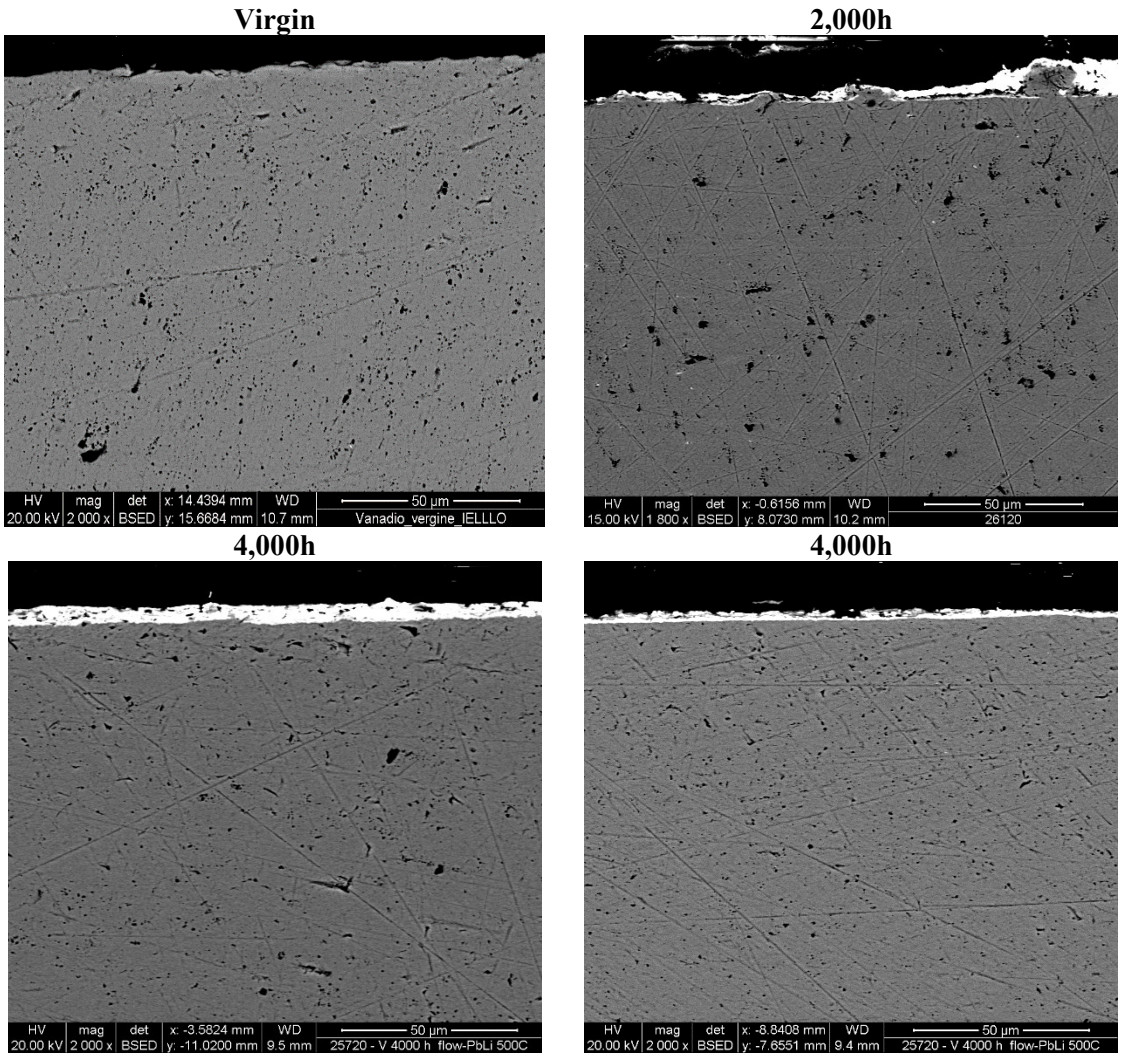

Figure 8: Cross-section SEM images at 1,800-2,000x magnification of V specimen as virgin and exposed for 2,000 and 4,000 h in flowing LiPb.

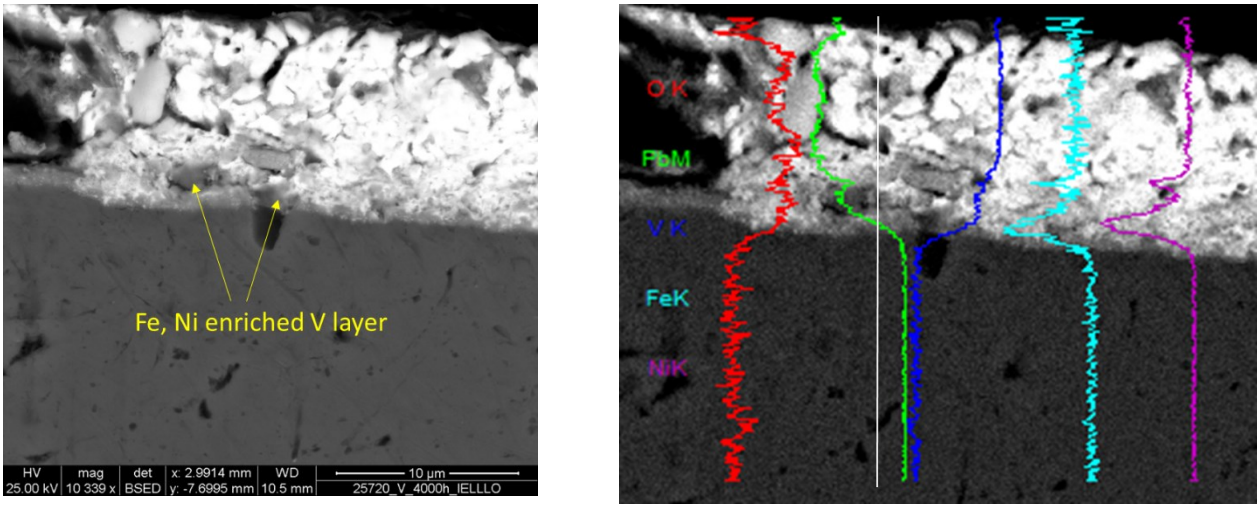

Figure 9: Cross-section SEM images of V specimen after 4,000 h and elemental line-scan by EDX.

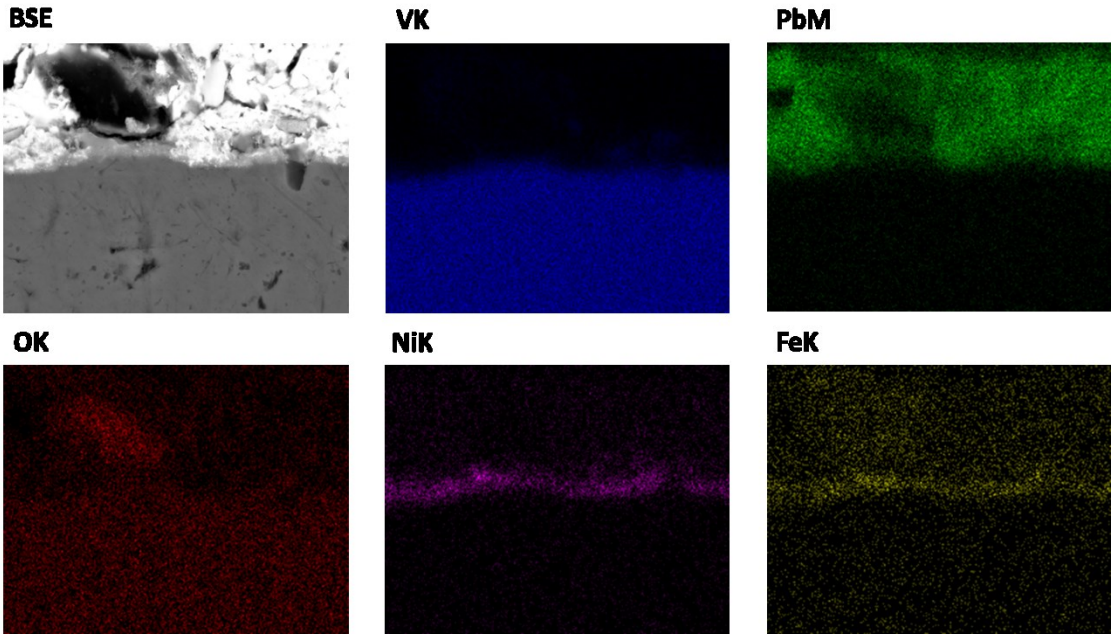

Figure 10: Cross-section SEM images of V specimen after 4,000 h and elemental maps by EDX.

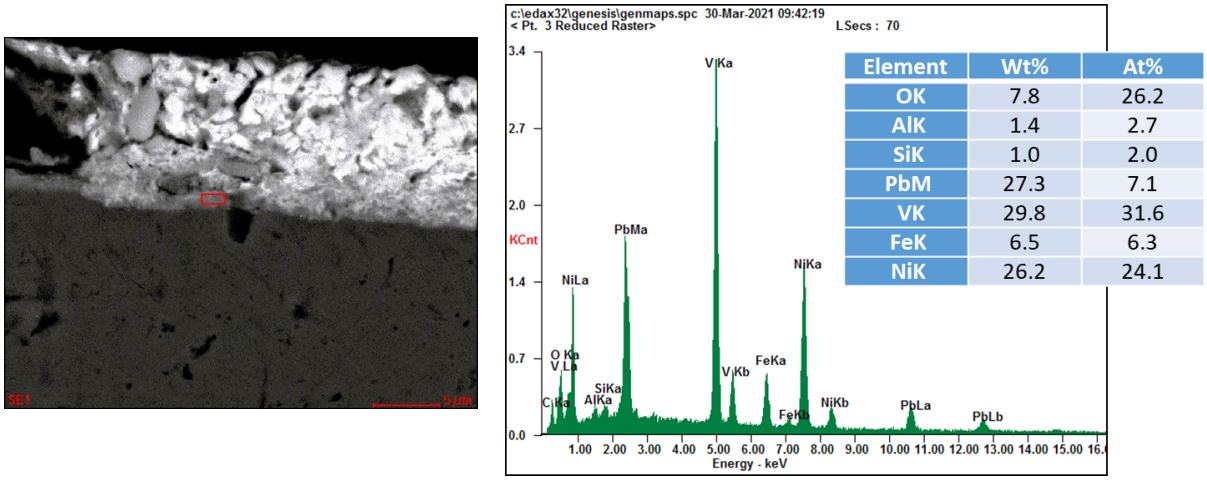

Element	Wt%	At%
OK	7.8	26.2
AlK	1.4	2.7
SiK	1.0	2.0
PbM	27.3	7.1
VK	29.8	31.6
FeK	6.5	6.3
NiK	26.2	24.1

Figure 11: Point EDX elemental composition on Fe, Ni enriched layer on V specimen after 4,000 h.

3.2.3 P22

Figure 12 shows cross-section SEM images at lower (2,000x) and higher (5,000x) magnification of P22 specimens after exposure in flowing LiPb for 4,000 h. The surface is affected by LiPb penetration with a depth ranging from 2 to 8 µm. Penetration of LiPb was previously detected for specimens exposed to 1,000 and 2,000 h with similar depths (up to 9 µm). No portions of detached specimen were found near the interface in the LiPb. The surface profile of the specimens appears to be similar between the various exposures and no significant increase of roughness was detected after 4,000 h.

For the surface examination, a portion of the specimen was cleaned with a soft solution of hydrogen peroxide, acetic acid and ethanol to not degrade the alloy (ratio 1:1:1 diluted up to 10% vol.). As detected also for shorter exposure times (1,000 and 2,000 h), significant Cr enrichment was found on

the samples surface after 4000 h of exposure, up to about 51% wt. (40% at.). This is confirmed by EDX maps of the elements (Figure 13) and by EDX line-scan (Figure 14). The enrichment was also confirmed by EDX surface analysis on a cleaned portion of the specimen (Figure 15).

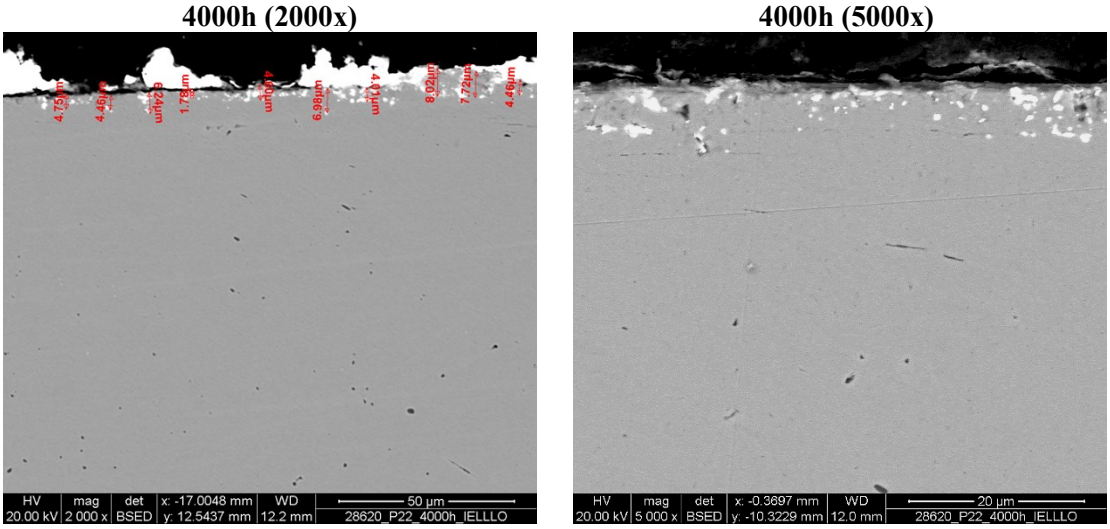

Figure 12: Cross-section SEM images at 2,000x and 5,000x magnification of P22 specimens exposed for 4,000 h in flowing LiPb.

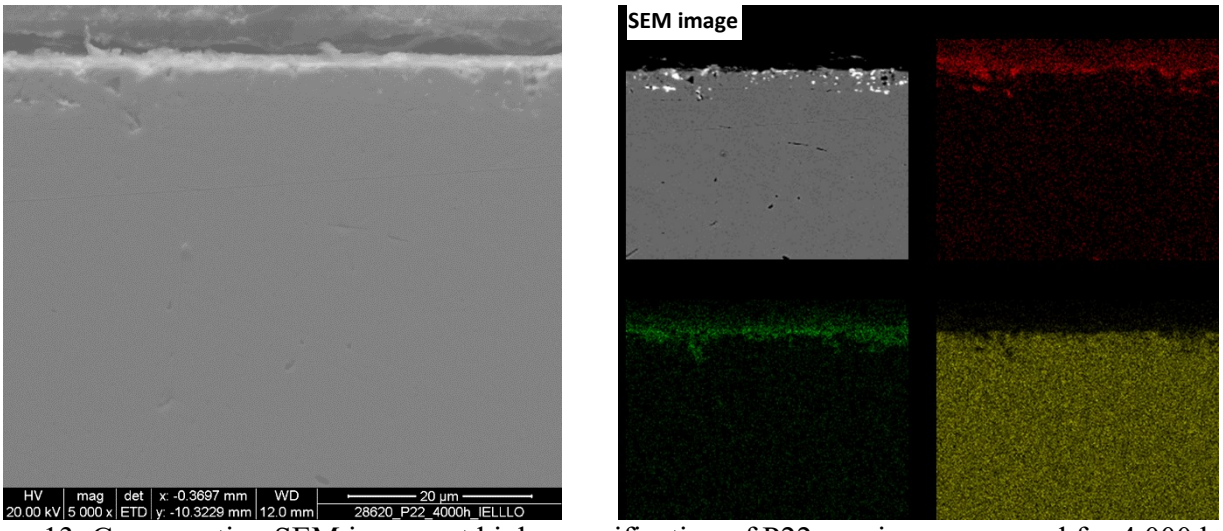

Figure 13: Cross-section SEM images at high magnification of P22 specimens exposed for 4,000 h and EDX maps showing Cr surface enrichment and LiPb penetration.

From SEM images at the lower magnification, the lines of the manufacturing are still visible, whereas at the higher magnification it is possible to observe the grainy appearance of the surface (also detected for 1,000 and 2,000 h exposed specimens). Cr enrichment is likely related to re-deposition of the corrosion products. As the LiPb in IELLLO presents significant contamination in the corrosion products coming from the loop piping (Fe, Cr, Ni), this re-deposition effect mostly comes from external Cr contamination. In addition, the surface EDX analysis performed on the exposed specimens at 1,000, 2,000 and 4,000 h shows that the surface Cr content increased with the exposure time (see Table 5),

suggesting that a sort of "covering" could have been occurred. Oxygen is also detected at the surface in small amounts and its presence could depend on the oxidation of the surface during the cleaning in the chemical solution.

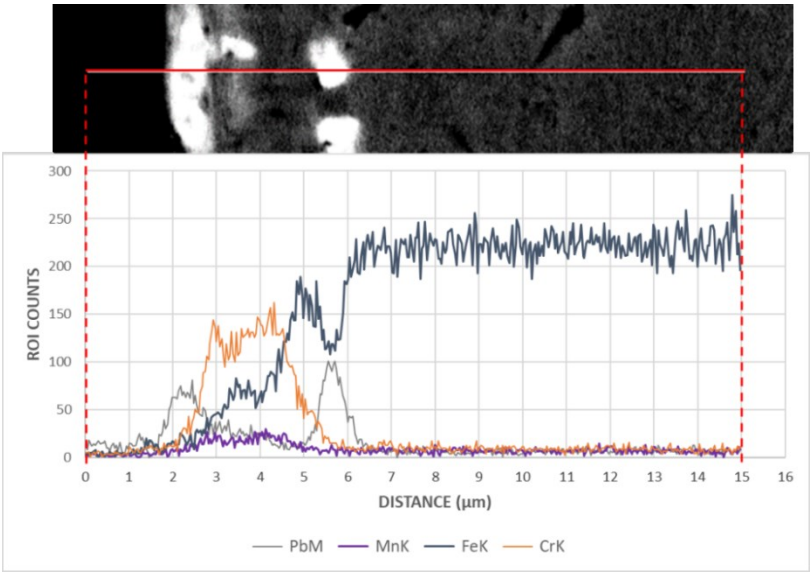

Figure 14: EDX line-scan of P22 specimens exposed for 4,000 h showing Cr surface enrichment and LiPb penetration.

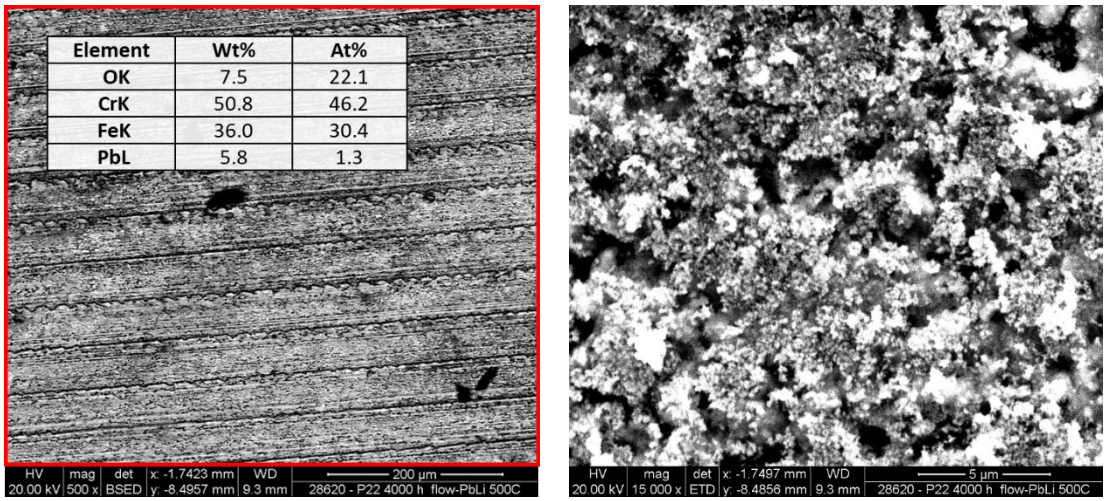

Figure 15: Surface SEM images at different magnification of P22 exposed to 4,000 h in flowing LiPb, with indication of the surface composition by EDX.

3.3 XRD analysis

3.3.1 Niobium

XRD spectra were collected for Nb specimens exposed to 2,000 and 4,000 h in flowing LiPb and are reported in Figure 16. The pattern for 2,000 h indicates the primary presence of Nb metal. Other very small peaks were detected in 2θ range 25-40° and find some agreement to compounds such as Fe, $NbNi_3$, $NbFe_2$ and NbO_2 in accordance with surface composition of Nb specimens.

The pattern for 4,000 h indicates again the primary presence of Nb metal and consistent peaks were found in high agreement to $NbNi_3$ compound. This is in accordance with surface composition of Nb specimens at 4,000 h which exhibit high surface Ni content (Figure 7).

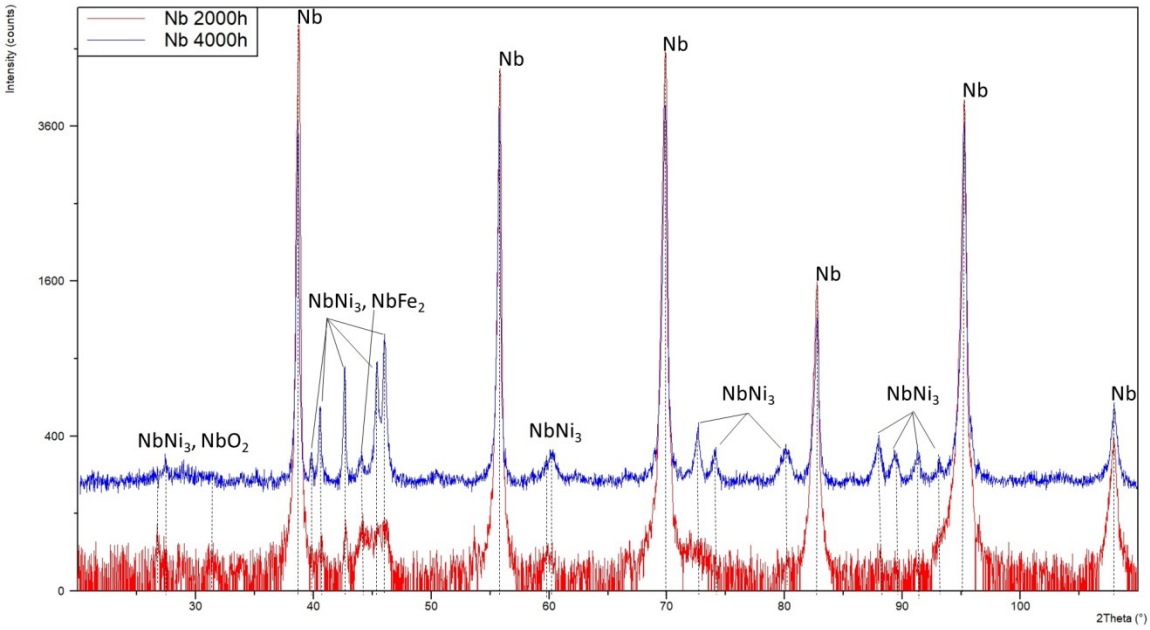

Figure 16: XRD pattern for Nb specimens exposed for 2000 h and 4000 h.

3.3.2 Vanadium

XRD spectrum was preliminary collected for 1,000 h specimen, that was partially cleaned on corrosive acetic acid and hydrogen peroxide solution (Figure 17). As the specimen conserved the intermetallic phase formed by interaction with Fe and Ni in most of the surface, XRD analysis was performed to identify potential compounds. The pattern for 1,000 h indicates the primary presence of V metal. Consistent peaks find agreement with Ni or Ni_3V compound, and other small peaks find relation to Fe and Pb.

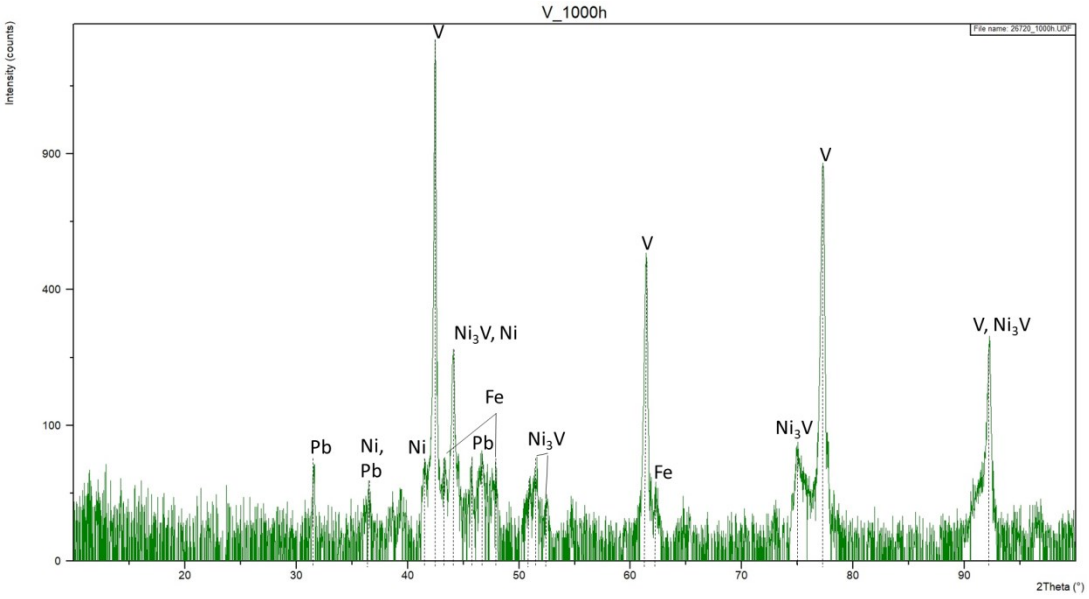

Figure 17: XRD pattern for V specimen exposed for 1,000 h (cleaned).

4. Discussion

4.1 Niobium

Corrosion of Nb was evaluated by weight loss after cleaning with chemical solution. Data obtained for 1,000, 2,000 and 4,000 h of exposure reveled no weight loss in flowing LiPb at 500°C. These results are in agreement with data obtained in static LiPb by Feuerstein and Grabner, which reported a low solubility of 0.053 ppmw at 600°C [7]. In this work, a slight increase of weight was detected and this may be related to the formation of a Fe, Ni enriched layer on the surface.

The examination of the profile interface of Nb after the various exposure times in flowing LiPb indicates that the roughness is globally conserved, but in some parts an increase was observed. This effect could be related to the formation of the new compound (Fe, Ni intermetallic) in the porosity and surface cavity at the interface, as the material presents a rough starting surface. The formation of an intermetallic layer on niobium was already observed in liquid Pb at 1000°C in presence of dissolved Ni, Cr and Fe in the melt [22].

The analysis of the composition of the Nb interface across the various exposure times shows a layer composed by Fe and mainly Ni on the surface. The layer formed is supposed to be thin and in some portions of the surface it was found to be detached in form of particles suspended in the solidified LiPb. The formation of surface compounds is also confirmed by the grainy/crystalline morphology of the surface after chemical cleaning. The surface composition, obtained after cleaning of the specimens for all the exposure times, showed a significant amount of Ni on the surface. A summary of the EDX surface composition over the exposure times is reported in Table 2. The content of Ni increased with the exposure time (from 4 to about 40% wt.) whereas the content of Fe decrease (from 8 to about 3% wt.). High amount of oxygen was found especially for 1,000 and 2,000 h of exposures.

Table 2: Surface composition of Nb specimens over the exposure times detected by EDX.

Time (h)	O		Nb		Ni		Fe	
	Wt. %	At. %	Wt. %	At. %	Wt. %	At. %	Wt. %	At. %
1,000	12	42	77	47	4	4	8	8
2,000	19	55	62	30	16	12	3	3
4,000	11	35	38	20	48	42	3	3

From EDX semi-quantitative composition it is difficult to state about the possible compound or compounds formed at the interface. In addition, there is the EDX limitation in detecting Li element, which may interact with the surface. By looking at phase diagrams, Nb element is prone to form a variety of intermetallics both with Ni and Fe [23][24] and isothermal sections at 450 and 500°C are available for ternary Nb-Ni-Fe phase diagram [25][26].

In addition, it is to consider the presence of oxygen, which may interact to form oxides. Nb-oxides (Nb_2O_5, NbO_2 and NbO) are thermodynamically instable in LiPb environment (see Ellingham diagram of Figure 18) and, if really present on the surface, they may be related to oxidation during draining in hot argon before extraction or due to the formation of more stable mixed oxides (such as LiNb oxides potentially forming by Li interaction). However, thermodynamic data of known LiNb oxides such as $LiNbO_3$ or Li_3NbO_5 are uncertain and data available in literature are not fully consistent to definitively assess the thermodynamic stability in LiPb (Figure 19).

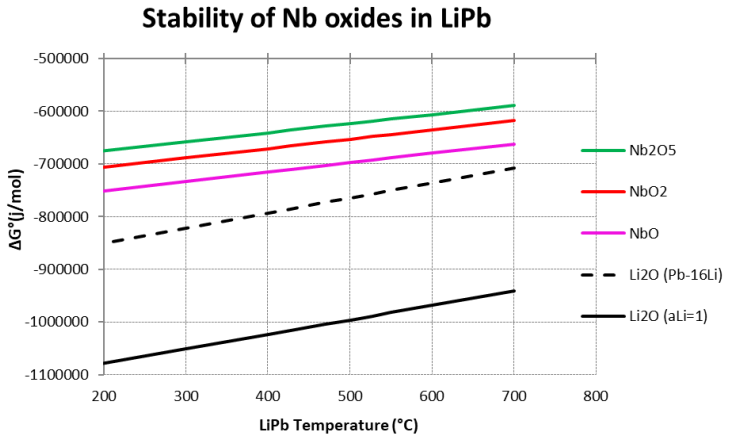

Figure 18: Ellingham diagram of Nb oxides in LiPb eutectic. Thermodynamic data for Nb oxides were taken from [27].

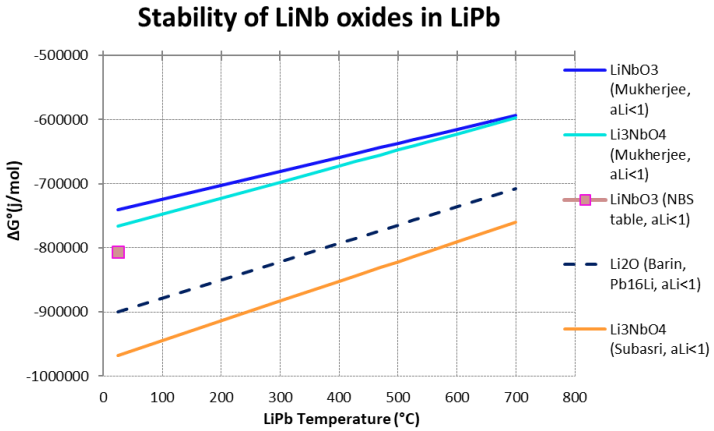

Figure 19: Ellingham diagram of LiNb oxides in LiPb eutectic. Thermodynamic data for LiNb oxides were taken from [28][29][30].

XRD spectra have then been performed on 2,000 and 4,000 exposed specimens in order to identify possible compounds. According to the spectra, Nb was the predominant phase in the 2,000 h specimen and traces likely related to $NbNi_3$ and Fe_2Nb were found. To the opposite, Ni_3Nb phase is consistent in the 4,000 h exposed specimen, in accordance with the increase of Ni content detected by surface EDX analysis in Table 2. The formed phases are in fairly agreement with ternary phase diagram section at 500°C (see Figure 20): at 1,000 and 2,000 h the stable phase are Nb with μ solid solution [31]. To the opposite, the surface enrichment of Ni stabilized the $NbNi_3$ phase at 4,000h, as detected in the XRD spectrum.

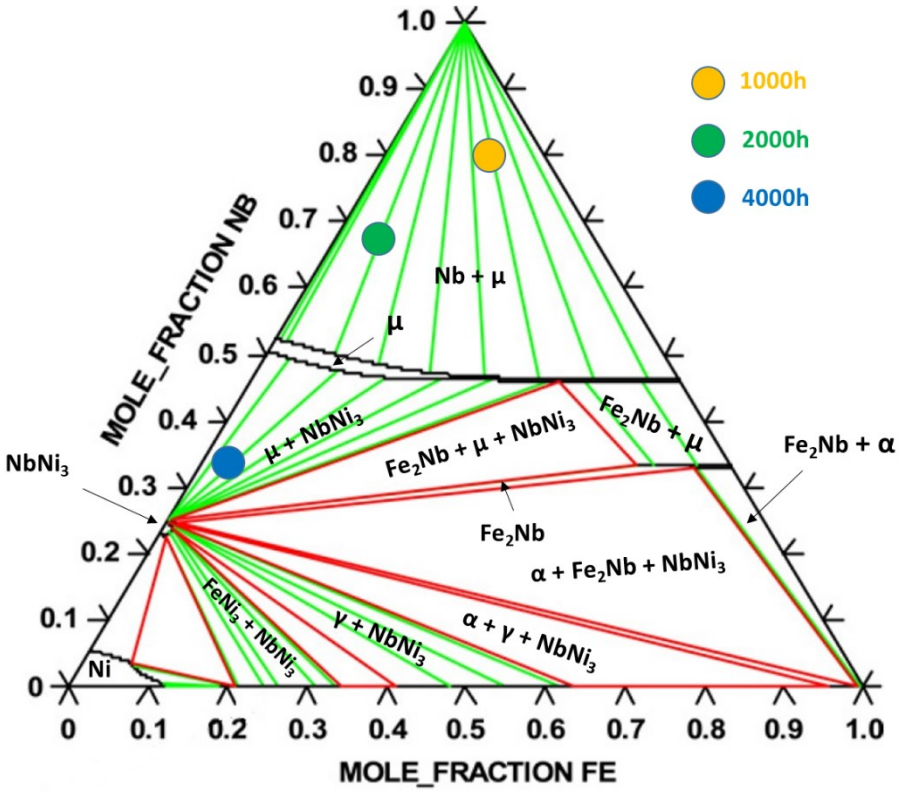

Figure 20: Ternary Nb-Ni-Fe phase diagram section at 500°C (figure adapted from [26] with permission from Elsevier under license 5240860644879). The points correspond to surface composition detected by EDX for the various exposure times.

4.2 Vanadium

The examination of the profile interface and the analysis of the chemical composition at the interface indicates that some corrosion has occurred. Going on with the exposures, the interface profile became smoother and the starting roughness of the specimens disappeared from cross-section analyses. In addition, a Fe and Ni enriched V layer was found at the interface in all the exposures, with a thickness of 1-2 µm max. This interaction is related to the formation of stable intermetallics or solid solutions with Fe and Ni, as shown in Fe-V and Ni-V phase diagrams [32][33][34]. Also traces of Al were found in the layer (see Figure 11) and Al is prone to form intermetallics with V [35]. The "smoothing" effect may be due to dissolution, or most likely to the formation of an intermetallic layer that tends to dissolve in LiPb. According to Feuerstein and Grabner, the solubility of V is reported to be quite low at 500°C (1.1 ppmw), suggesting that the formation of the intermetallic compounds may have the primary role over the corrosion.

Corrosion of V alloys was studied in static and flowing LiPb in past by Adelhelm et al. [9] and Borgstedt et al. [10], who detected the interaction of V with contaminants. According to the work by Adelhelm, V-3Ti-1Si alloy was tested in static LiPb inside stainless steel capsules at 357 and 547 °C for about 1000 h. The adherent LiPb layer on the specimens was not removed for weight loss evaluation, and only element composition analysis was performed on the specimens. At 357 °C the surface was basically unaffected and conserved the starting roughness after the exposure, whereas a corrosion attack was detected at 547 °C as a consequence of the interaction with Fe, Cr and Ni

contaminants (coming from the corrosion of the steel capsules). The original surface and starting roughness was not anymore recognized after the test and the interface changed into a bubble-shape layer. Borgstedt tested V-3Ti-1Si alloy in flowing LiPb at 550°C up to 3687 h. V alloy specimens exhibited a weight gain ascribable to an interaction with Fe contaminant and the formation of a thin Fe-composed metal layer on the surface. The formation of an intermetallic layer on V was also observed in liquid Pb at 1000°C in presence of dissolved Ni, Cr and Fe in the melt [22].

Preliminary data here reported confirm previous results by Adelheim and Borgstedt. A corrosion attack on V specimens is identified as a consequence of the interaction with contaminants and formation of Fe, Ni enriched V layer. A summary of the chemical composition of the layer for the various exposure times is reported in Table 3. By neglecting Pb content on the surface (not expected to interact with V [36]), the trend of the elements indicates that Ni slightly accumulates with the exposure time whereas Fe content is high at low exposure time (1,000 h) and then decreases. Oxygen is constant over time and may be related to oxidation of the adherent LiPb on the surface, since oxygen peak has not been detected through the line-scan across the surface at 2,000 and 4,000 h and single V-oxides are not stable in LiPb (Figure 21). However, potential interaction of O with V, Li and contaminants to form stable oxides in LiPb eutectic is not to be excluded a priori in the form of traces.

Table 3: Surface composition of V specimens over the exposure times detected by EDX.

Time (h)	O		V		Ni		Fe		Pb	
	Wt. %	At. %	Wt. %	At. %	Wt. %	At. %	Wt. %	At. %	Wt. %	At. %
1,000[a]	8	33	19	24	16	17	9	11	47	14
2,000[a]	11	44	14	17	17	18	4	4	54	17
4,000[b]	8	33	30	33	27	25	7	5	28	7

a) Surface EDX on uncleaned specimen
b) Cross EDX at the interface

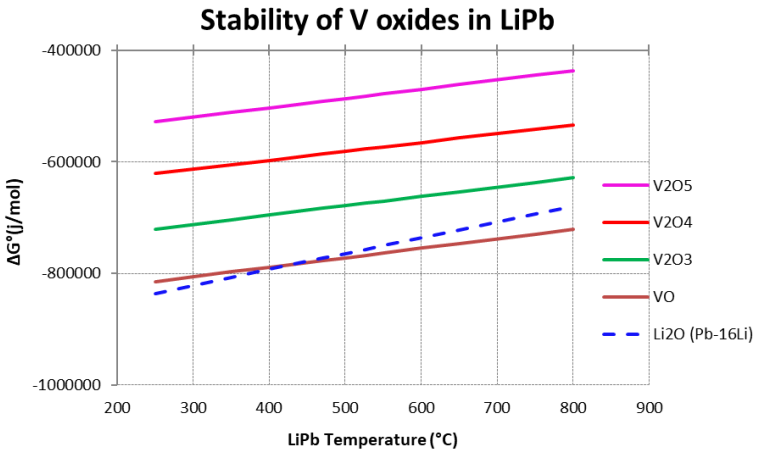

Figure 21: Ellingham diagram of V oxides in LiPb eutectic. Thermodynamic data for V oxides were taken from [27].

Unfortunately, no isothermal sections around 500 °C are available for ternary phase diagram V-Fe-Ni and so no prediction about the stability of the phases can be performed considering the chemical

compositions detected for 1,000, 2,000 and 4,000 h of exposure. However, the XRD spectrum obtained for the 1,000 h exposed specimen indicates the formation of a Ni-V intermetallic phase and the presence of Ni and Fe, which may form solid solutions. In particular, Ni_3V and Ni_2V have peaks in accordance with the present spectrum. According to binary Ni-V phase diagram, formation of these intermetallics is possible in the range of Ni content between 20-50% at. (cf. [33]).

4.3 P22 steel

A penetration of LiPb at the interface was observed from the analysis of the P22 profile over the exposure times. The values of LiPb penetration are very similar for the different times and ranges between 2 and 9 µm (Table 4). As the internal bulk composition profile did not change significantly over the exposure times at the interface (selective leaching of element was not detected) and no detachments were detected, it is to suppose that uniform dissolution and erosion mostly proceeds with a currently unknown corrosion rate.

Table 4: LiPb penetration in P22 specimens for the various exposure times up to 4000h.

Time (h)	Min. Penetration (µm)	Av. Penetration (µm)	Max. Penetration (µm)
1,000	1.7	4.7	9.0
2,000	2.9	5.9	8.8
4,000	1.8	4.6	8.0

From the point of view of the surface chemical composition, it was found a significant enrichment of Cr over the various exposures. This strong enrichment is likely due to re-deposition of corrosion products and mostly related to contamination of the LiPb in the loop. Reasonably, this enrichment would have influenced the weight loss by a gain contribution if corrosion rate by weight loss had been evaluated. Moreover, surface Cr enrichment and re-deposition increases with the exposure times, as shown in Table 5 reporting the general trends of O, Cr and Fe evaluated by EDX after cleaning of the specimens. Presence of O should be related to the oxidation of the surface with the chemical solution.

Table 5: Surface composition of P22 specimens over the exposure times detected by EDX.

Time (h)	O		Cr		Fe	
	Wt. %	At. %	Wt. %	At. %	Wt. %	At. %
virgin	-	-	2.14	-	95.8	-
1,000	3	10	30	29	66	60
2,000	9	25	47	40	45	36
4,000	8	22	54	46	38	31

5 Conclusions

In this paper results about the exposure of materials in flowing LiPb at 500°C up to 4,000 h are reported. The materials under investigation were: Nb, V and P22 ferritic steel. For Nb specimens, weight loss analysis was performed to evaluate the corrosion rate. For V specimens, weight loss measurements after chemical cleaning are not effective in determining the corrosion rate as vanadium

is rapidly attack by typical oxidizing chemical solutions used to remove LiPb residuals, and only qualitative characterization is reported. For P22 specimens, only qualitative characterization is presented as well.

Nb specimens do not show relevant weight loss after 4,000 h. A slight increase of weight was detected, related to the formation of a thin layer made of Fe, Ni contaminants present in LiPb alloy. After 4,000 h of exposure, the interaction with Ni is remarkable and $NbNi_3$ compound was detected on the surface.

V specimens exhibited a smoother surface after the exposure and the original surface finishing state was no longer identified after 4,000 h. In addition, corrosion was identified due to an interaction with Fe and Ni contaminants. The formation of this compound needs to be deeper investigated but preliminary XRD analysis up to 1,000 h indicates formation of a Ni-V intermetallic.

The applicability of Nb and V as membrane materials for the Permeator Against Vacuum technology could be questioned by their interaction with contaminants and by the formation of intermetallics that may affect the permeability to tritium. This point requires additional investigation to be fully clarified.

P22 specimens undergo LiPb penetration at the interface and uniform corrosion spread above the surface. Strong Cr enrichment was found in the near interface, likely related to re-deposition phenomena of contaminants on the surface. Tests in controlled environment should be performed in the future in order to investigate exhaustively the corrosion behavior of this material.

Acknowledgements

This work has been carried out within the framework of the EUROfusion Consortium and has received funding from the Euratom research and training programme 2014-2018 and 2019-2020 under grant agreement No. 633053. The views and opinions expressed herein do not necessarily reflect those of the European Commission. The work of A. Venturini is financially supported by a EUROfusion Engineering Grant.

The authors are grateful to Mr. Daniel Gianotti, Mr. Lorenzo Laffi, Mr. Claudio Lenzi, Mr. Demis Santoli, Mr. Valerio Sermenghi and Mr. Massimo Valdiserri for their help at various stages of this experimental campaign.

References

[1] A. Del Nevo et al., Recent progress in developing a feasible and integrated conceptual design of the WCLL BB in EUROfusion project, Fus. Eng. Des. 146 B (2019), 1805-1809.

[2] M. Utili et al., Tritium extraction from HCLL/WCLL/DCLL LiPb BBs of DEMO and HCLL TBS of ITER, IEEE Transactions on Plasma Science 47 (2) (2019),1464-1471.

[3] S. A. Steward, Review of Hydrogen Isotope Permeability Through Materials, UCRL-53441 https://doi.org/10.2172/5277693.

[4] F. Papa et al., Engineering design of a Permeator Against Vacuum mock-up with niobium membrane, Fus. Eng. Des. 166 (2021), 112313.

[5] F. Papa et al., Manufacturing of a Permeator Against Vacuum mock-up with niobium membrane, submitted to the Nuclear Materials and Energy.

[6] B. Garcinuño et al., Design and fabrication of a Permeator Against Vacuum prototype for small scale testing at Lead-Lithium facility, Fus. Eng. Des. 124 (2017), 871-875.
[7] H. Feuerstein et al., Compatibility of refractory metals and beryllium with molten Pb-17Li, Journal Nucl. Mat. 233-237 (1996), 1383-1386.
[8] H. Grabner et al., Compatibility of metals and alloys in liquid Pb-17Li at temperatures up to 650°C, Journal Nucl. Mat. 155-157 (1988) 702-704.
[9] Ch. Adelhelm et al., Analysis of V-3Ti-1Si alloy after exposure to Pb-17Li, Journal Nucl. Mat. 155-157 (1988) 698-701.
[10] H.U. Borgstedt et al., Vanadium alloy for the application in a Liquid Metal Blanket of a fusion reactor, Journal Nucl. Mat. 155-157 (1988) 690-693.
[11] J. Konys et al., Flow rate dependent corrosion behavior of Eurofer steel in Pb–15.7Li, Journal Nucl. Mat. 417 (2011), 1191–1194.
[12] H. Borgstedt et al., Corrosion of stainless steel in flowing- LiPb eutectic, Journal Nucl. Mat. 141-143 (1986), 561-565.
[13] J. Konys and W. Krauss, Corrosion and precipitation effects in a forced-convection Pb–15.7Li loop, Journal Nucl. Mat. 442 (2013), S576–S579.
[14] G. Benamati et al., Mechanical and corrosion behaviour of EUROFER 97 steel exposed to Pb–17Li, Journal Nucl. Mat. 307–311 (2002), 1391–1395.
[15] R. Mozzillo et al., Integration of LiPb loops for WCLL BB of European DEMO, Fus. Eng. Des. 167 (2021), 112379.
[16] M. Tarantino et al., Fusion technologies development at ENEA Brasimone Research Centre: Status and perspectives, Fus. Eng. Des. 160 (2020), 112008.
[17] S. Bassini et al., oral contribution at the ICFRM-20 virtual conference, 24-29 October 2021.
[18] Y. Çengel and J. Cimbala, Fluid mechanics : fundamentals and applications, 2006, McGraw-Hill.
[19] A. Venturini et al., Experimental and RELAP5-3D results on IELLLO (Integrated European Lead Lithium LOop) operation, Fus. Eng. Des. 123 (2017), 143-147.
[20] A. Venturini et al., Experimental Qualification of New Instrumentation for Lead-Lithium Eutectic in IELLLO Facility, Fus. Eng. Des. 156 (2020), 111683.
[21] A. Venturini et al., Experimental investigation on HCLL-TBS In-box LOCA, Fus. Eng. Des. 146 A (2019), 173-177.
[22] O. I. Eliseeva, Formation of intermetallic layers on the surface of refractory metals in a lead melt under conditions of mass transfer, Materials Science 35, No. 2 (1999), 252-258.
[23] E. Paul, L. J. Swartzendruber, The Fe-Nb (Iron-Niobium) System, Bulletin of Alloy Phase Diagrams 7 No. 3 (1986) 248-253.
[24] A. Nash, P. Nash, The Nb-Ni (Niobium-Nickel) System, Bulletin of Alloy Phase Diagrams 7 No. 2 (1986) 124-129.
[25] V. Raghavan, Fe-Nb-Ni (Iron-Niobium-Nickel), Journal of Phase Equilibria and Diffusion 31 No. 2 (2010) 180-183.
[26] M. Mathon et al., CALPHAD-type assessment of the Fe-Nb-Ni ternary system, CALPHAD: Computer Coupling of Phase Diagrams and Thermochemistry 33 (2009), 136-161.
[27] I. Barin and G. Platzki, Thermochemical Data of Pure Substances, Third ed. VCH, Weinheim; New York (1995).
[28] S. Mukherjee et al., Thermodynamic studies on $LiNbO_3$(s) and Li_3NbO_4(s) using Knudsen effusion quadrupole mass spectrometry and differential scanning calorimetry, Journal of Alloys and Compounds 714 (2017) 681-686.
[29] R. Subasri and O. M. Sreedharan, Thermodynamic stability of Li_3NbO_4 by emf measurements using a novel composite electrolyte, Solid State Ionics 93 (1997) 341-346.
[30] D. D. Wagman et al., The NBS table of chemical thermodynamic properties, Journal of Physical and Chemical Reference Data, Volume 11 Supplement No 2 (1982).
[31] M. Takeyama et al., Phase equilibria among γ, Ni_3Nb-δ and Fe_2Nb-ε phases in Ni-Nb-Fe and Ni-Nb-Fe-Cr systems at elevated temperatures, Superalloys 718, 625, 706 and Various Derivatives, Edited by E. A. Loria, TMS (The Minerals. Metals & Materials Society), 2001.
[32] H. Okamoto, Fe-V (Iron-Vanadium), Journal of Phase Equilibria and Diffusion Vol. 27 No. 5 2006.
[33] J. F. Smith et al. The Ni-V (Nickel-Vanadium) System, Bulletin of Alloy Phase Diagrams Vol. 3 No. 3 (1982), 342-348.
[34] V. Raghavan, Fe-Ni-V (Iron-Nickel-Vanadium), Journal of Phase Equilibria Vol. 15 No. 6 (1994), 630.
[35] H. Okamoto, Al-V (Aluminum-Vanadium), Journal of Phase Equilibria and Diffusion Vol. 33 No. 6 (2012), 491.

[36] J. F. Smith, The Pb-V (Lead-Vanadium) System, Bulletin of Alloy Phase Diagrams Vol. 2 No. 2 (1981), 209-210.